Journal of Electroanalytical Chemistry 906 (2022) 116024

Contents lists available at ScienceDirect

Journal of Electroanalytical Chemistry

journal homepage: www.elsevier.com/locate/jelechem

Cobalt single atom sites in carbon aerogels for ultrasensitive enzyme-free electrochemical detection of glucose

Yaya Song [a], Ting He [a,*], Yulin Zhang [b], Chunyang Yin [a], Yang Chen [a], Qiming Liu [c], Yi Zhang [a,*,d], Shaowei Chen [c,*]

[a] Hunan Provincial Key Laboratory of Micro & Nano Materials Interface Science, School of Chemistry and Chemical Engineering, Central South University, Changsha, Hunan 410083, China
[b] School of Laboratory Medicine, Hubei University of Chinese Medicine, 16 Huangjia Lake West Road, Wuhan, Hubei 430065, China
[c] Department of Chemistry and Biochemistry, University of California, 1156 High Street, Santa Cruz, CA 95064, United States
[d] Key Laboratory of Materials Processing and Mold (Zhengzhou University), Ministry of Education, Zhengzhou 450002, China

ARTICLE INFO

Keywords:
Biomass hydrogel
Carbon aerogel
Single atom catalyst
Nonenzymatic detection
Glucose

ABSTRACT

Enzyme-free electrochemical glucose sensors have been attracting extensive attention, due to high sensitivity, excellent stability, and low cost, as compared to the conventional counterparts based on biological enzymes such as glucose oxidase. Within this context, development of low-cost, high-performance electrode catalysts represents a critical first step, and nanocomposites with atomically dispersed metal sites have emerged as viable candidates. In this study, nitrogen-doped carbon aerogel (NCA) embedded with CoN_x sites is derived pyrolytically from biomass hydrogels and serves as an electrode catalyst for the detection of glucose. The three-dimensional porous skeletons of NCA help disperse the Co single atom sites and facilitate the mass transfer during electrochemical reaction. Theoretical calculations reveal that the single metal sites (CoN_3 and CoN_4) at the edge of nanopores show optimal adsorption towards glucose, and likely make a dominant contribution to the high activity in glucose detection. In electrochemical measurements, the NCA-Co based, enzyme-free glucose sensor shows a detection limit of 0.1 μM, with a wide linear range from 0.5 μM to 6 mM, good stability, high selectivity and excellent reproducibility. Notably, this sensing platform also exhibits an excellent performance in determining the glucose contents in artificial saliva and human serum samples, indicating great potential for practical applications.

1. Introduction

Glucose is an indispensable nutrient for metabolism in the body, and abnormality of the glucose level can lead to various diseases [1]. A low level of glucose will cause hypoglycemia as well as insulin shock (diabetic coma), whereas an excess amount of glucose can lead to diabetes [2]. Currently there are more than 400 million diabetes patients worldwide [1,3]. At present, there is no effective way to cure diabetes, and one effective strategy to control diabetes is to closely monitor and carefully control the glucose level in the body [4]. It has been advised that diabetes patients should test their blood glucose levels several times a day [5]. Due to the huge demand for self-monitoring glucose levels, a wide variety of glucose sensors have been developed, based on acoustic, mass, optical, and electrical sensing principles [6–9]. Of these, electrochemical sensors for glucose detection have been attracting particular attention, which entail both enzyme-based and enzyme-free detecting platforms, due to simple, fast, and real-time operation, low detection limit, and miniaturized apparatus [10]. Since the first enzyme-based glucose electrochemical sensor by Clark and Lyons in 1962 [11], significant progress has been made, especially, with regards of sensitivity and selectivity [12]. One major limitation of such glucose sensors is that the enzyme activity can be significantly affected by the environmental changes, such as temperature, humidity, and pH [13]. To mitigate this issue, development of enzyme-free sensors represents an attractive alternative, due to the high sensitivity and diversity, good stability, and low cost [14].

In enzyme-free electrochemical sensors, functional nanocomposites are commonly used as the electrode catalysts. For instance, precious metal-based nanomaterials, such as Pt and Au, have shown high catalytic efficiency toward glucose oxidation [15,16]; yet widespread application is impeded by their high cost and easy deactivation [14]. Thus, significant research has been devoted to nonprecious metals-based catalysts for enzyme-free glucose detection, such as Ni, Co, Cu, Mn, Fe, and their alloys, due to their low cost, good selectivity

* Corresponding authors.
E-mail addresses: heting891020@csu.edu.cn (T. He), yzhangcsu@csu.edu.cn (Y. Zhang), shaowei@ucsc.edu (S. Chen).

https://doi.org/10.1016/j.jelechem.2022.116024
Received 21 November 2021; Received in revised form 17 December 2021; Accepted 5 January 2022
Available online 8 January 2022

and remarkable stability [3,17]. Among these, Co-based nanocomposites are of particular interest, which exhibit appropriate adsorption interaction between the Co sites and oxygen-containing groups, and hence high catalytic activity towards glucose detection [1]. The electrocatalytic activity can be further enhanced when the metals are atomically dispersed into a carbon skeleton, forming single atom catalysts (SACs) [18–20]. A range of carbon derivatives have been used as the structural scaffold, such as graphene [21], carbon nanotubes [22], carbon nitride [23], and porous carbon [24], primarily due to their high electrical conductivity, and ready doping with select heteroatoms for the stabilization of SACs [25–28]. In such SACs, the exact atomic configuration of the metal sites dictates the electrocatalytic activity, and porosity of the composites impacts the accessibility of the catalytic active sites and mass transfer of important reactant species [29,30]. Carbon aerogels represent a unique option, which can be readily derived from biomass hydrogels via controlled pyrolysis [18,31].

In the present study, *N*-doped carbon aerogels (NCA) embedded with Co single atoms (denoted as NCA-Co) were prepared pyrolytically by using low-cost gelatin hydrogels as the precursors. The obtained NCA-Co nanocomposites exhibited unique structural characteristics, such as microporous defects and nanowrinkles, where Co single atoms were anchored and stabilized. Theoretical studies suggested that these SAC sites facilitated the adsorption and oxidation of glucose. In fact, electrochemical measurements showed high activity towards glucose detection, with a detection limit of 0.1 μM and a wide linear range from 0.5 μM to 6 mM, excellent stability, high selectivity and reproducibility. Additionally, the NCA-Co based sensor exhibited a remarkable performance in the detection of glucose in artificial saliva and human serum samples, indicating great potential for practical applications.

2. Experimental section

2.1. Chemicals

Gelatin, cobalt(II) acetate tetrahydrate ($Co(Ac)_2{\blacksquare}4H_2O$), ferrous chloride tetrahydrate ($FeCl_2{\blacksquare}4H_2O$), nickel(II) acetate tetrahydrate ($Ni(Ac)_2{\blacksquare}4H_2O$), zinc(II) acetate tetrahydrate ($Zn(Ac)_2{\blacksquare}4H_2O$), and SiO_2 nanoparticles were purchased from Aladdin Reagents (Shanghai, China). Sodium hydroxide (NaOH), 1,10-phenanthroline monohydrate (PM), acetylene black, 5% Nafion solution, and glucose were obtained from Sigma Aldrich (America). All other reagents were of analytical grade, and ultrapure water (MillQ, 18.2 MΩ cm) was used throughout this study.

2.2. Characterization

Scanning electron microscopy (SEM) and transmission electron microscopy (TEM) images were acquired on a Hitachi S-4800 field-emission SEM and FEI Talos F200S field-emission electron microscope, respectively. Inductively coupled plasma-optical emission spectrometry (ICP-OES) analysis was performed with a SPECTRO BLUE SOP instrument. X-ray diffraction (XRD) patterns were collected with a D/max 2550 X-ray powder diffractometer. X-ray photoelectron spectroscopic (XPS) measurements were conducted with an ESCALAB 250Xi instrument. Nitrogen adsorption/desorption isotherms were acquired with a Micromeritics ASAP2460 instrument. X-ray absorption spectroscopy (XAS) measurements were performed in the Shanghai Synchrotron Radiation Facility in the fluorescence mode at room temperature (298 K).

2.3. Sample preparation

NCA-Co nanocomposites were prepared by following a procedure reported previously [18,28,31]. In brief, 24 mg of PM was dispersed in 200 μL of $Co(Ac)_2{\blacksquare}4H_2O$ (0.2 M) under sonication to produce an orange $Co(PM)_3^{2+}$ solution. Separately, 60 mg of gelatin, 30 mg of SiO_2, and 2.7 mL of water were mixed in a screw-cap vial under magnetic stirring in a 60 °C water bath for 10 min, into which were then added 200 μL of the 0.2 M $Co(PM)_3^{2+}$ and 80 μL of 1.0 M $Zn(Ac)_2$ solution. The obtained hydrogels (denoted as $G_{Si\text{-}Zn}$/Co-PM) were subject to freezing-thawing three times, before being pyrolyzed at 900 °C for 3 h in a tube furnace under a constant flow of 97% Ar + 3% H_2 at the heating rate of 5 °C min^{-1}. After being cooled down naturally to room temperature, the product was etched by HF to remove SiO_2 nanoparticles, affording NCA-Co.

NCA-Fe and NCA-Ni were prepared in the same manner except that $FeCl_2{\blacksquare}4H_2O$ and $Ni(Ac)_2{\blacksquare}4H_2O$ were used instead as the meal source. Metal-free carbon aerogel (NCA) was also prepared in the same manner but without the addition of any metal-PM complex.

2.4. Preparation of glucose sensors

1 mg of the NCA-Co powders obtained above was dispersed into a 1 mL solution that contained 475 μL of H_2O, 475 μL of ethanol, and 50 μL of a 5% Nafion solution. 10 μL of the produced ink was dropcast onto the surface of a clean glassy carbon electrode (GCE, 3 mm in diameter) and dried in air. The modified GCE was used as the working electrode, a saturated calomel electrode (SCE) as the reference electrode, and a platinum wire as the auxiliary electrode. All electrochemical measurements were performed with a CHI 440 electrochemical workstation.

2.5. Detection of glucose

Cyclic voltammetry (CV) was used to test the electrochemical oxidation activity, and chronoamperometry to detect glucose at the applied potential of +0.3 V, with glucose of various concentrations added to a 0.1 M NaOH aqueous solution. The test of each sample was repeated three times, from which the standard deviation was estimated. To evaluate the performance of the NCA-Co sensor in the determination of glucose in practical samples, an artificial saliva solution was prepared, which contained 9 g L^{-1} NaCl, 0.4 g L^{-1} KCl, 0.2 g L^{-1} $NaHCO_3$, and 0.2 g L^{-1} $CaCl_2{\cdot}6H_2O$ [32]. Clinical serum samples were also obtained from Huangjiahu School Hospital of Hubei University of Traditional Chinese Medicines, where proteins were precipitated out by the addition of 2 mL of acetonitrile to 1 mL of the serum. The supernatants were collected by centrifugation for 15 min and dried at 50 ℃ in nitrogen, before being re-dissolved in 1 mL of a phosphate buffer solution (PBS). 5 μL of the obtained solution was then diluted with 4950 μL of 0.1 M NaOH for glucose detection.

3. Results and discussion

3.1. Structural characterization

The preparation of NCA-Co nanocomposites is schematically illustrated in Fig. 1a, where three-dimensional gelatin-zinc hydrogel was employed as the precursor, with the Co-PM complex and SiO_2 nanoparticles as the metal source and porogen, respectively. From Fig. 1b, the freeze-dried hydrogel precursors can be seen to exhibit a honeycomb structure with rich macropores. By subsequent pyrolysis and acid etching, the hydrogels were effectively transformed into porous carbon aerogels embedded with Co single atoms (NCA-Co). This is indeed confirmed in TEM measurements (Fig. S1a), where the obtained carbon aerogel can be seen to possess a continuous, porous carbon skeleton free of metal or metal oxide nanoparticles. A similar morphology was observed with the metal-free NCA sample (Fig. S2). Furthermore, from the STEM image in Fig. 1c, one can see a number of isolated white spots (red circles), suggesting the formation of atom-

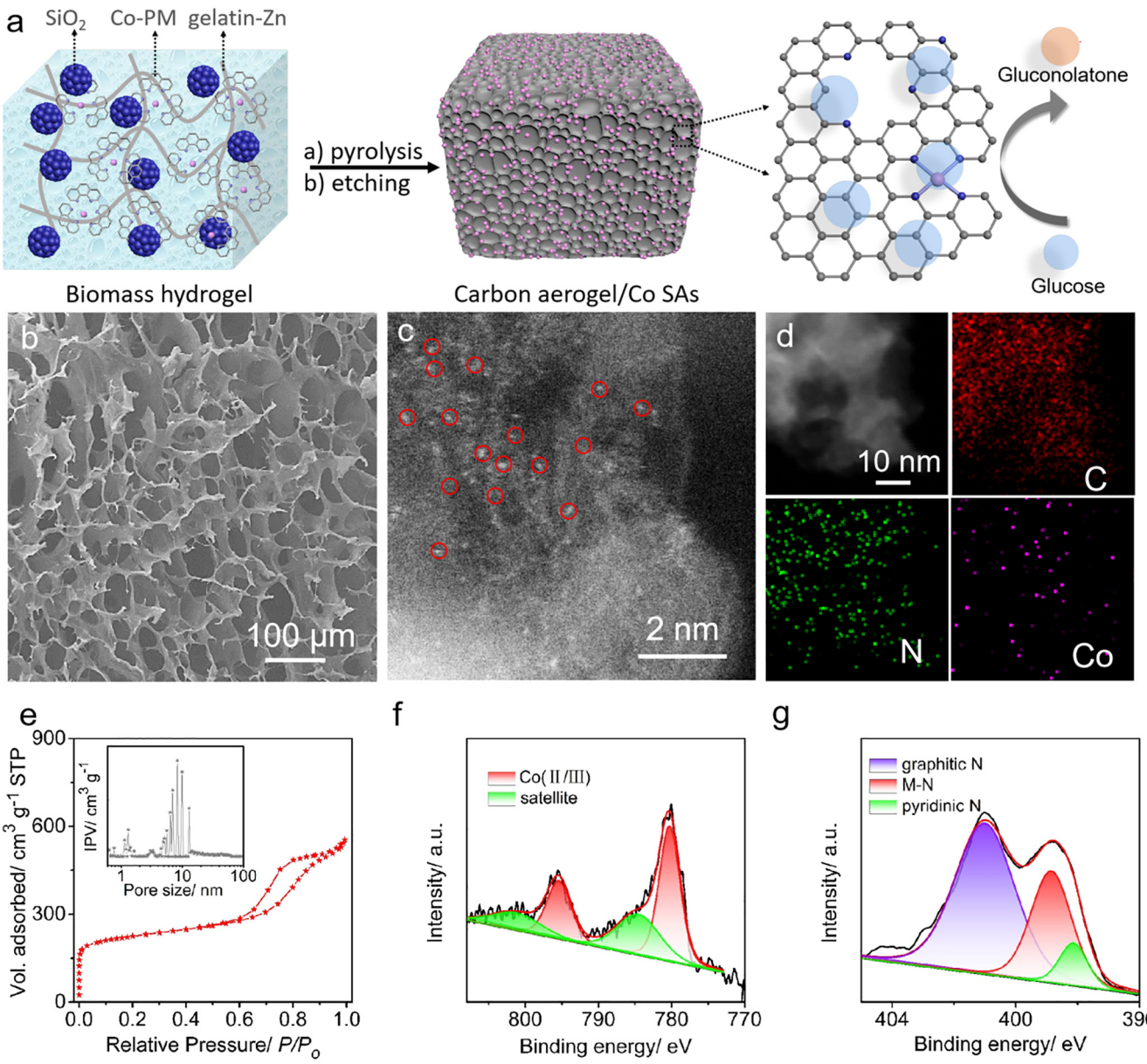

Fig. 1. (a) Schematic of the preparation of NCA-Co aerogels derived from biomass hydrogels. (b) SEM of the $G_{Si\text{-}Zn}$/Co-PM hydrogel precursor. (c) STEM image and (d) elemental maps of NCA-Co composites. (e) Nitrogen adsorption/desorption isotherm of NCA-Co composites. Inset is the corresponding pore size distribution. High-resolution XPS scans of the (e) Co 2P, and (f) N 1s electrons of NCA-Co composites. Black curves are experimental data and colored peaks are deconvolution fits.

ically dispersed metal species in the carbon matrix. Indeed, elemental mapping analysis based on energy-dispersive X-ray spectroscopy (EDS, Fig. 1d and S3) shows that Co, along with N and O, was distributed rather evenly across the carbon matrix without apparent agglomeration. These observations are consistent with results obtained previously in the preparation of NCA aerogels embedded with isolated Fe atoms [18].

From Fig. 1e and inset, the NCA-Co aerogels can be seen to exhibit a nitrogen adsorption/desorption isotherm with a type IV hysteresis loop, and possess a hierarchical pore structure with a high surface aera of 827.2 $m^2\ g^{-1}$, consisting primarily of mesopores (5 to 10 nm) and micropores (0.5 to 2 nm), in agreement with results from TEM measurements (Fig. S1b). These porous defects are anticipated to facilitate the anchoring of single metal atom sites, especially at the pore edges. Additionally, XRD measurements yield only two broad peaks at $2\theta = 24.91^\circ$ and 43.66° (Fig. S4), due to the (0 0 2) and (1 0 1) diffractions of graphitic carbon (PDF card #65-6212), respectively, suggesting successful graphitization of the hydrogel into aerogel; and the fact that no other diffraction feature can be resolved is consistent with the atomic dispersion of Co into the carbon skeleton. In XPS measurements of the NCA-Co sample (Fig. S5), the C 1s, N 1s, O 1s, and Co 2p electrons can be readily resolved at ca. 284, 400, 530 and 780 eV, respectively; and from the integrated peak areas, the elemental composition can be estimated to be ca. 88.2 wt% C, 6.0 wt% O, 4.6 wt% N and 1.2 wt% Co (Table S1). Note that the Co content was consistent with that obtained from ICP-OES measurements (Table S1). From the high-resolution scan of the O 1s spectrum in Fig. S6, two peaks can be resolved at 531.41 and 532.62 eV, due to C═O and C—O/O—H, respectively [28].

Notably, the absence of Co-O species at ca. 530 eV is consistent with results from TEM and XRD measurements where no metal oxide nanoparticles were detected. For the Co 2p spectrum (Fig. 1f), decon-

volution yields a doublet at 780.27 and 795.40 eV, along with satellite peaks at 784.50 and 801.20 eV, which can be assigned to Co(II) [33]; and in the N 1 s spectrum (Fig. 1g), three N species can be identified at 401.03 eV for graphitic N, 398.23 eV for pyridinic N, and 398.85 eV for metal-N (M−N) [33]. This suggests that Co atoms are most likely chelated with N atoms in the form of CoN_x embedded in the carbon aerogel skeleton. Intriguingly, the ratio between N in M−N moieties (0.9 at%) and Co (0.25 at%) in the NCA-Co sample is estimated to be 3.6:1 (Tables S1 and S2), suggesting that the Co atoms were dispersed in the carbon aerogel in the forms of ca. 60% CoN_4 and 40% CoN_3.

The chemical state and coordination environment of the Co centers in NCA-Co were then investigated by X-ray absorption near-edge structure (XANES) and extended X-ray absorption fine structure (EXAFS) measurements. From Fig. 2a, one can see that the Co K-edge of NCA-Co is close to that of CoO, but deviates markedly from that of Co foil [34], suggesting a Co center with a valence state of about +2 [35]. From the R-space EXAFS profile (Fig. 2b), NCA-Co can be seen to exhibit a main peak at about 1.4 Å and a shoulder at 2.3 Å, which can be respectively assigned to the Co-N coordination of the first shell and Co-C coordination of the second shell [36]. From the fitting results of the EXAFS data (Fig. 2c and S7, Table S3), the Co-N coordination number was estimated to be 3.6 for NCA-Co, suggesting a mixture of CoN_4 and CoN_3 moieties, in good agreement with results from XPS measurements (Fig. 1f-g). Taken together, these results suggest three possible metal sites, namely, CoN_4 in the basal plane, as well as CoN_4 and CoN_3 on the edge of nanopores.

3.2. Theoretical investigations

In alkaline media, the Incipient Hydroxyl Oxide Adatom Model (IHOAM) is commonly used to describe the interaction of glucose molecules with active sites [37,38], where OH species adsorb onto the metal sites. To examine whether this IHOAM can be used for SAC metal sites, NCA-Fe and NCA-Ni carbon aerogels were also synthesized in the same fashion and their interactions with glucose was analyzed and compared with that of NCA-Co [39]. Fig. S8 shows the optimal structures of these single metal sites within the basal plane of the carbon scaffold. From the calculated adsorption energy of glucose in Fig. S9 (details in the Supplementary Information) and the detection sensitivity of glucose (the response signal per 100 μM of glucose) in Fig. S10, one can see that the adsorption energy shows a positive correlation with the sensitivity (Fig. S11), and the Co atom sites exhibit the optimal adsorption energy and best electrochemical activity. These results confirm the excellent applicability of IHOAM to single metal sites.

Notably, in addition to basal CoN_4 sites (Fig. S8a), NCA-Co also contains CoN_4 and CoN_3 moieties at the nanopore edges (Fig. 3a-3c), as suggested by the above XAS studies (Fig. 2). The adsorption of glucose onto the metal sites were then examined (Figs. S12 and S13). From Table S4, one can see that the Co-O bond length is 1.884 Å for basal CoN_4, which increases to 1.964 Å for CoN_4 and 1.891 Å for CoN_3 at the nanopore edge. Such a discrepancy of the Co-O bond length suggests that the formation of microporous defects and reduced coordination of the metal atoms impact the charge density of the Co atom and hence the interaction with glucose. Glucose molecules can adsorb onto the metal sites by hydrogen bonding interaction, as shown in Fig. 3d-f [40]. Note that the calculated adsorption energy is all neg-

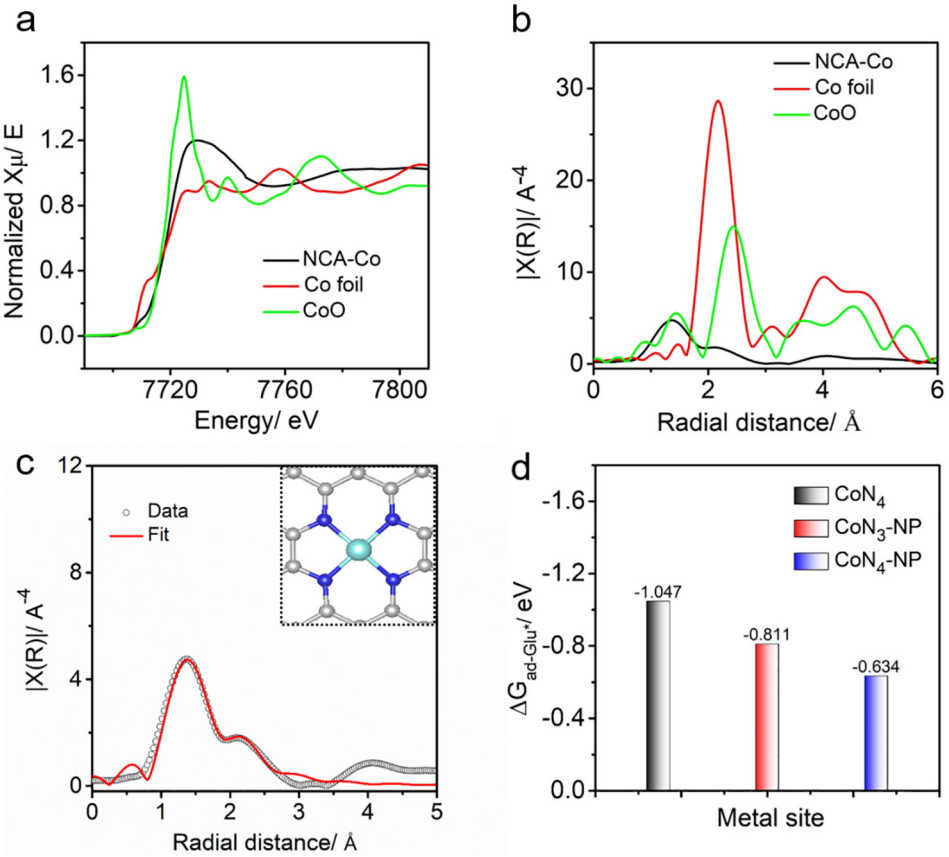

Fig. 2. (a) Co K-edge XANES and (b) R-space EXAFS spectra of NCA-Co, Co foil, and CoO. (c) EXAFS and fitting curves for NCA-Co. Inset is the structure of a CoN_4 site. (d) Adsorption energy of glucose over OH-adsorbed CoN_4 on the basal plane, CoN_3 and CoN_4 on the nanopore edge (CoN_3-NP and CoN_4-NP).

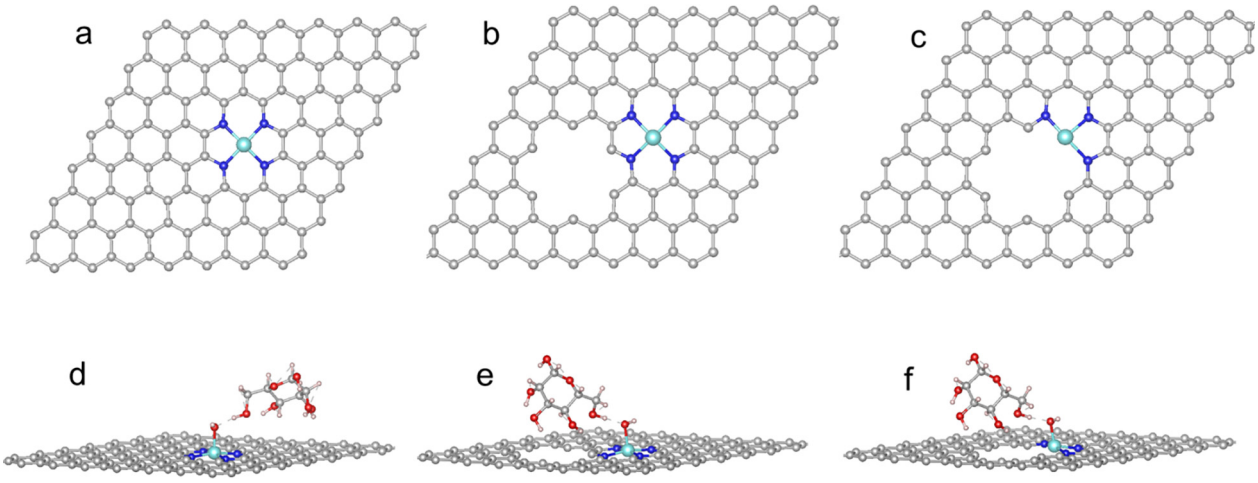

Fig. 3. Top views of the optimized structures of (a) basal CoN_4, (b) CoN_4 and (c) CoN_4 at the nanopore edge. Adsorption of a glucose molecule over OH-adsorbed (d) basal CoN_4, (e) CoN_4 and (f) CoN_3 on the nanopore edge.

ative and varies in the following order, basal CoN_4 (−1.047 eV) < nanopore-edge CoN_3 (−0.811 eV) < nanopore-edge CoN_4 (−0.634 eV) (Fig. 2d), and the last two actually resemble those of highly active noble metal sites (ca. −0.7 eV) [37,40]. That is, the metal sites on the edge of nanopores likely made a dominant contribution to the high electrocatalytic activity of glucose detection, as observed below [41].

3.3. Electrochemical behaviors and glucose detection

To demonstrate the application of the NCA-Co aerogels for non-enzymatic glucose sensing, the nanocomposites were deposited onto a GCE surface and examined by electrochemical measurements. Fig. 4a shows the cyclic voltammograms (CVs) of the bare GCE, NCA modified GCE (designated as NCA/GCE), and NCA-Co modified GCE (designated as NCA-Co/GCE) in 0.1 M NaOH at the scan rate of 0.05 V s^{-1}. One can see that NCA-Co/GCE exhibited only a featureless response in the absence of glucose. Yet, with the addition of 5 mM glucose, whereas there remained no obvious voltametric feature at the GCE and NCA/GCE electrodes, a pair of voltametric peaks appeared at +0.35 and +0.28 V. This is due to the redox reaction of glucose [42], indicating the unique catalytic activity of NCA-Co/GCE in the oxidation of glucose in NaOH. The discrepancy of the catalytic activity can also be observed in chronoamperometric measurements. From Fig. 4b, one can see that at the applied potential of +0.3 V, the bare GCE exhibited essentially zero current response with the successive additions of 100 μM glucose, the NCA/GCE electrode showed a slight increment of ca. 0.05 μA upon each addition, whereas the current increment (ca. 1 μA) was almost 20 times greater with the NCA-Co/GCE electrode. This indicates that the CoN_x moieties played the key role in the electrocatalytic oxidation of glucose [43].

To obtain the optimal performance for glucose detection, the NaOH concentration and the applied potential were optimized at 0.1 M and 0.3 V, respectively (Fig. S14 and S15). Fig. 4c depicts the oxidation current profile upon the injections of various concentrations of glucose into a 0.1 M NaOH solution. The i-t segment for the addition of 0.5–50 μM glucose was magnified and shown in the inset to Fig. 4c. One can observe that the oxidation current increment increases as the concentration of added glucose increases from 0.5 μM to 6 mM. Within the glucose concentration range of 0.5 to 1000 μM, the oxidation current increment exhibits a good linear relationship with the glucose concentration (Fig. 4d and 4e), which can be fitted by the equation of I (μA) = 0.0078C + 0.0496 (C represents the glucose concentration, μM) with the regression coefficient of R^2 = 0.997. A different linear correlation can be found at higher glucose concentrations of 1 to 6 mM (Fig. 4f), I (μA) = 0.001C + 6.4 (R^2 = 0.990). The low detection limit was estimated to be 0.1 μM (S/N = 3), much lower than a range of enzyme-free glucose sensors reported in the literature (Table 1). The wide linear range of this NCA-Co/GCE sensor was likely ascribed to the three-dimensional porous *N*-doped carbon structure which facilitated the accessibility of the catalytically active sites, whereas the low detection limit was due to CoN_x moieties that were electrocatalytically active towards glucose oxidation.

3.4. Reproducibility, stability and selectivity

The reproducibility of the NCA-Co/GCE sensor toward glucose detection was then evaluated. Firstly, 5 NCA-Co/GCE electrodes were prepared in the same manner and their chronoamperometric responses toward glucose were separately tested and compared. From Fig. S16, one can see that the relative standard deviations (RSDs) among the 5 electrodes is only 3.19%, indicating excellent reproducibility of the NCA-Co/GCE platform. Fig. 5a shows the test results of an NCA-Co/GCE electrode stored in air at room temperature for up to a week. It can be seen that even after a week's storage, the current response toward the 100 μM glucose still retained 92.8% of the initial value, indicating remarkable stability of the fabricated electrode.

The selectivity of the NCA-Co/GCE electrode toward glucose detection was also studied. Most interfering substances co-existing with glucose in human blood can be easily oxidized, but their normal physiological levels are significantly lower than the glucose concentration [49]. We opted to add 100 μM of glucose and 200 μM of various interfering substances (i.e., L-histidine, L-alanine, L-ascorbic acid, urea, dopamine, L-glutamic acid, and quinidine) to exaggerate the impacts. Interestingly, despite the abnormally high concentrations of the interfering substances, their additions introduced only a negligible increment of the current response, in comparison to that with glucose (Fig. 5b). Furthermore, the addition of high concentration NaCl (50 mM) and NH_4Cl (50 mM) also produced only minimal impacts. Taken together, these results highlight the excellent selectivity of NCA-Co/GCE towards glucose sensing.

3.5. Analysis of practical samples

Significantly, the NCA-Co/GCE sensor also exhibited an excellent performance in detecting glucose in practical samples, such as artificial saliva and human serum samples. Two different concentrations of glucose (5 and 100 μM) were added to the artificial saliva, and the glucose

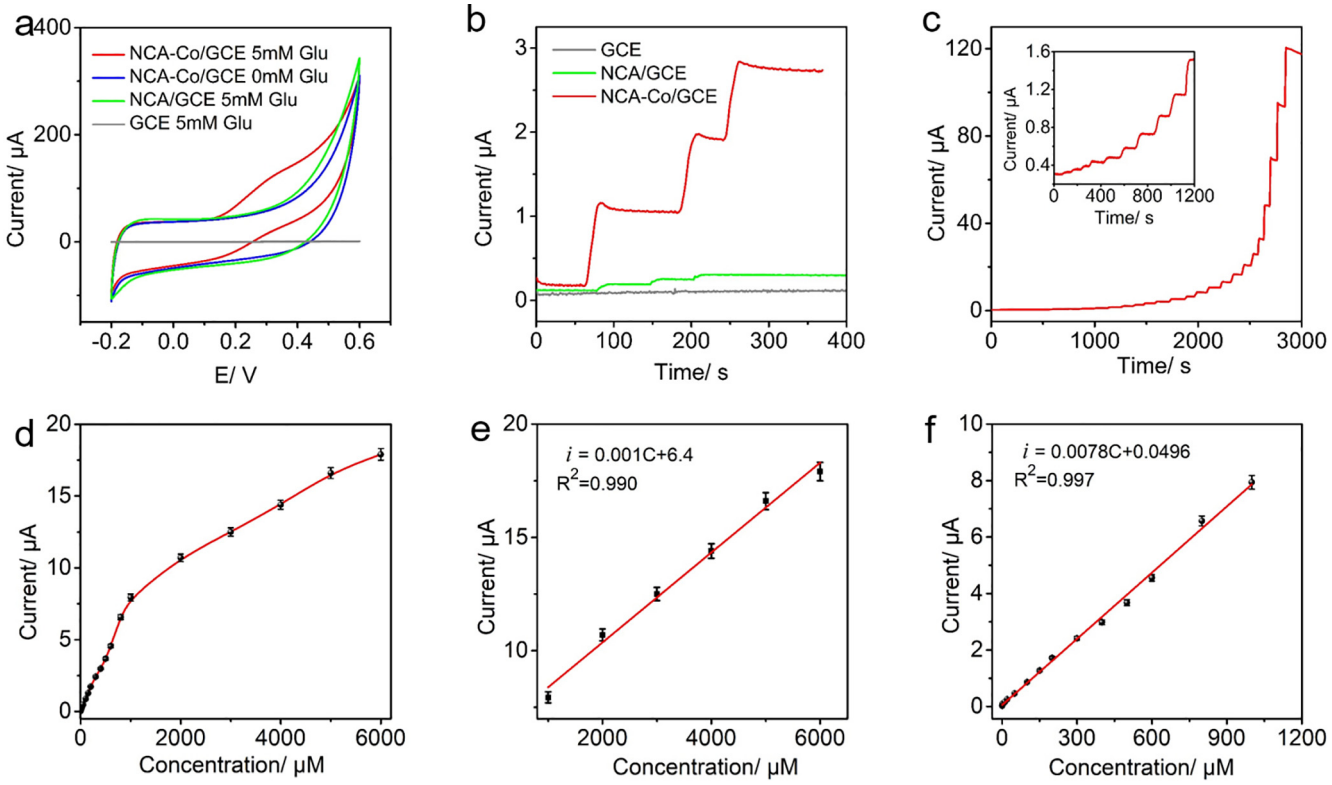

Fig. 4. (a) Cyclic voltammograms in 0.1 M NaOH at the scan rate 50 mV s^{-1} of NCA-Co/GCE in the absence and presence of 5 mM glucose, NCA/GCE and bare GCE in the presence of 5 mM glucose. (b) Chronoamperometric profiles of different modified electrodes at the applied potential of +0.3 V with the successive additions of 100 μM glucose into 0.1 M NaOH. (c) Chronoamperometric curve of the NCA-Co/GCE electrode upon the successive addition of glucose at various concentrations (0.5, 1, 2, 10, 20, 50, 100, 150, 200, 300, 400, 500, 600, 800, 1000, 2000, 3000, 4000, 5000, 6000 μM) into a 0.1 M NaOH solution at the applied potential of +0.3 V. Inset is the magnified segment for the glucose concentration range of 0.5 to 100 μM. (d) Current signals at different glucose concentrations (Table S5) and the corresponding linear correlation between the oxidation current increment and glucose concentration in the range of (e) 0.5–1000 μM and (f) 1000–6000 μM.

Table 1
List of electrochemical glucose sensors in terms of electrode materials, linear range and limit of detection in chronoamperometric analysis.

Electrode Materials	Linear range	Limit of Detection (μM)	Potential (vs Ag/AgCl)	Electrolyte	Ref.
NCA-Co carbon aerogel	0.5 μM–6 mM	0.1	+0.30 V	0.1 M NaOH	This work
$Co_2N_{0.67}$ nanosheets	10 μM–8 mM	0.1	+0.55 V	0.1 M NaOH	[14]
Cu-Co/RGO	1 μM–4 mM	0.15	+0.40 V	0.1 M NaOH	[2]
CoPc/graphene	10 μM–5 mM	0.67	+0.70 V	0.1 M NaOH	[1]
Ag-CuO nanoparticles	10 μM–28 mM	0.76	+0.60 V	0.1 M NaOH	[10]
Ni-MOF	5 μM–7.4 mM	1.5	+0.55 V	0.1 M NaOH	[44]
Ni 1D/C_{60}	10 μM–11 mM	4.3	+0.57 V	0.1 M NaOH	[17]
Cu_2O@ZIF-67	10 μM–16.3 mM	6.5	+0.55 V	1 M KOH	[45]
Cu nanowires-MOFs-GO	20 μM–26.6 mM	7.0	+0.30 V	0.1 M PBS	[46]
AuCu alloy NPs	250 μM–10 mM	16.62	+0.60 V	0.1 M NaOH	[47]
Cu@C core–shell nanocube	40 μM– 40 mM	21.35	+0.60 V	0.4 M NaOH	[48]

concentrations were quantitatively assessed by the NCA-Co/GCE sensor at 4.86 and 98.9 μM, corresponding to a recovery value of 97.2% and 98.9%, respectively, with an RSD of 2.86% and 5.40% (Table S6 and Fig. 4c).

Further tests were carried out with clinical human serum samples in 0.1 M NaOH. From the results in Table S7 and Fig. 4d, one can see that the RSDs of the 8 human serum samples were all under 5%, and the measurement results were all very close to those obtained with a commercial glucometer, with a recovery rate between 94% and 105%. These results indicate good potential of the NCA-Co/GCE sensor for practical applications (Table S8).

4. Conclusions

In this study, carbon aerogels embedded with Co single atoms (NCA-Co) were prepared by a facile pyrolysis procedure using biomass hydrogel as the precursor. With a highly porous structure, the NCA-Co composite showed an apparent electrocatalytic activity towards glucose oxidation, due to the formation of CoN_4 and CoN_3 moieties on the edge of micropores. This unique property can be exploited for the non-enzymatic detection of glucose, with a low detection limit of 0.1 μM, wide linear range, and excellent good stability. In addition, the NCA-Co/GCE platform exhibited high selectivity and excellent reproducibility, and demonstrated an excellent performance in the detection of glucose in practical samples, such as artificial saliva and

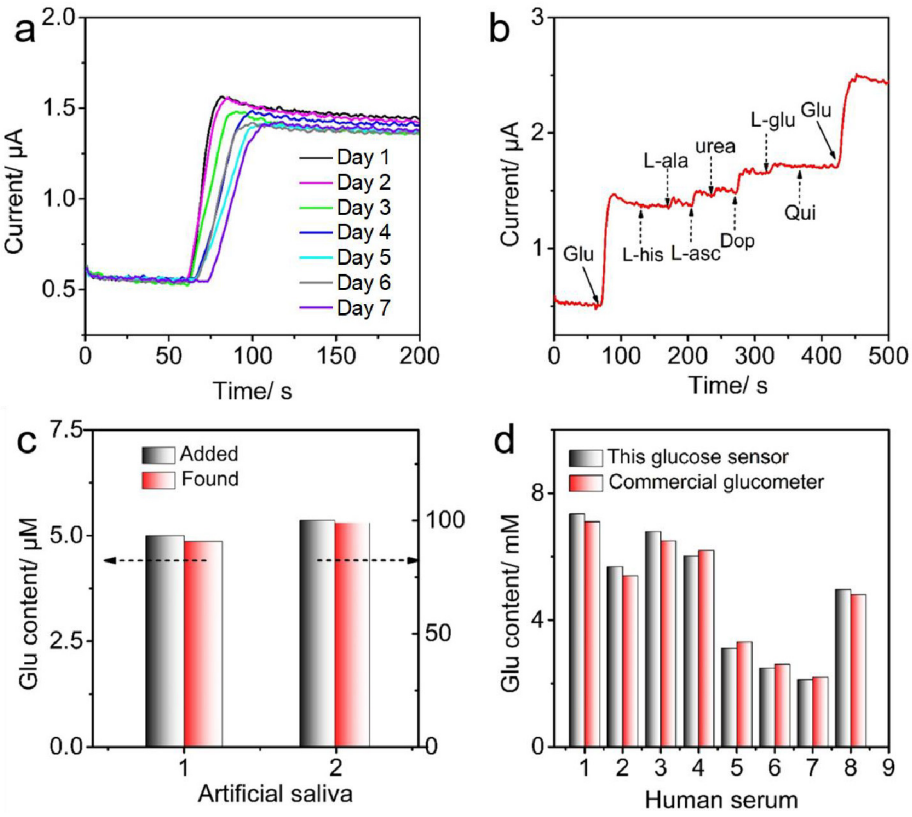

Fig. 5. (a) Chronoamperometric profiles of the NCA-Co/GCE electrode stored in ambient for up to a week with the addition of 100 μM glucose. (b) Chronoamperometric response of the NCA-Co/GCE electrode upon the addition of different substances (glucose, Glu; L-histidine, L-his; L-alanine, L-ala; L-ascorbic acid, L-asc; urea; dopamine, Dop; L-glutamic acid, L-glu; and quinidine, Qui). Determination of (c) glucose in artificial saliva and (d) clinical human serum samples by NCA-Co/GCE.

human serum samples, in comparison to results from a commercial glucometer. Results from this study highlight the significance of carbon aerogels with atomically dispersed metal atoms in the development of glucose sensors.

CRediT authorship contribution statement

Yaya Song: Investigation, Formal analysis. **Ting He:** Conceptualization, Funding acquisition, Project administration, Resources, Writing – review & editing. **Yulin Zhang:** Investigation, Data curation, Formal analysis. **Chunyang Yin:** Data curation, Formal analysis. **Yang Chen:** Data curation, Formal analysis. **Qiming Liu:** Data curation, Formal analysis. **Yi Zhang:** Conceptualization, Funding acquisition, Project administration, Resources, Writing – review & editing. **Shaowei Chen:** Conceptualization, Funding acquisition, Project administration, Resources, Writing – review & editing.

Declaration of Competing Interest

The authors declare that they have no known competing financial interests or personal relationships that could have appeared to influence the work reported in this paper.

Acknowledgments

This work is supported in part by the National Science Foundation (CHE-1900235 and CHE-2003685). Y. Z. acknowledged support from the National Natural Science Foundation of China (21972169, 21773311) and Hunan Provincial Science and Technology Plan Project (2019TP1001). Ting He thanks the Postdoctoral Research Foundation of Central South University (140050038); Yaya Song supported by the Fundamental Research Funds for the Central Universities of Central South University (1053320210029). The authors thank eceshi (www.eceshi.com) and High-Performance Computing Center of CSU.

Appendix A. Supplementary data

Supplementary data to this article can be found online at https://doi.org/10.1016/j.jelechem.2022.116024.

References

[1] S. Chaiyo, E. Mehmeti, W. Siangproh, T.L. Hoang, H.P. Nguyen, O. Chailapakul, K. Kalcher, Non-enzymatic electrochemical detection of glucose with a disposable paper-based sensor using a cobalt phthalocyanine–ionic liquid–graphene composite, Biosens. Bioelectron. 102 (2018) 113–120.
[2] K. Justice Babu, S. Sheet, Y.S. Lee, G. Gnana kumar, Three-dimensional dendrite cu–co/reduced graphene oxide architectures on a disposable pencil graphite electrode as an electrochemical sensor for nonenzymatic glucose detection, ACS Sustain Chem. Eng. 6 (2) (2018) 1909–1918.
[3] D.-W. Hwang, S. Lee, M. Seo, T.D. Chung, Recent advances in electrochemical non-enzymatic glucose sensors – a review, Anal. Chim. Acta 1033 (2018) 1–34.
[4] A.J. Bandodkar, S. Imani, R. Nuñez-Flores, R. Kumar, C. Wang, A.M.V. Mohan, J. Wang, P.P. Mercier, Re-usable electrochemical glucose sensors integrated into a smartphone platform, Biosens. Bioelectron. 101 (2018) 181–187.
[5] K. Tian, M. Prestgard, A. Tiwari, A review of recent advances in nonenzymatic glucose sensors, Mater. Sci. Eng.: C 41 (2014) 100–118.
[6] J. Luo, P. Luo, M. Xie, K. Du, B. Zhao, F. Pan, P. Fan, F. Zeng, D. Zhang, Z. Zheng, G. Liang, A new type of glucose biosensor based on surface acoustic wave resonator using Mn-doped ZnO multilayer structure, Biosens. Bioelectron. 49 (2013) 512–518.
[7] H. Yuan, W. Ji, S. Chu, S. Qian, F. Wang, J.-F. Masson, X. Han, W. Peng, Fiber-optic surface plasmon resonance glucose sensor enhanced with phenylboronic acid modified Au nanoparticles, Biosens. Bioelectron. 117 (2018) 637–643.

[8] N.S. Galenkamp, M. Soskine, J. Hermans, C. Wloka, G. Maglia, Direct electrical quantification of glucose and asparagine from bodily fluids using nanopores, Nat. Commun. 9 (2018) 4085.

[9] D. Chen, H. Li, X. Su, N. Li, Y. Wang, A.C. Stevenson, R. Hu, G. Li, A wireless-electrodeless quartz crystal microbalance method for non-enzymatic glucose monitoring, Sens. Actuators B: Chem. 287 (2019) 35–41.

[10] D. Xu, C. Zhu, X. Meng, Z. Chen, Y. Li, D. Zhang, S. Zhu, Design and fabrication of Ag-CuO nanoparticles on reduced graphene oxide for nonenzymatic detection of glucose, Sens. Actuators B: Chem. 265 (2018) 435–442.

[11] L.C. Clark Jr., C. Lyons, Electrode systems for continuous monitoring in cardiovascular surgery, Ann. N. Y. Acad. Sci. 102 (1962) 29–45.

[12] S. Radhakrishnan, H.-Y. Kim, B.-S. Kim, A novel CuS microflower superstructure based sensitive and selective nonenzymatic glucose detection, Sens. Actuators B: Chem. 233 (2016) 93–99.

[13] V. Veeramani, R. Madhu, S.-M. Chen, P. Veerakumar, C.-T. Hung, S.-B. Liu, Heteroatom-enriched porous carbon/nickel oxide nanocomposites as enzyme-free highly sensitive sensors for detection of glucose, Sens. Actuators B: Chem. 221 (2015) 1384–1390.

[14] T. Liu, M. Li, P. Dong, Y. Zhang, L. Guo, Design and facile synthesis of mesoporous cobalt nitride nanosheets modified by pyrolytic carbon for the nonenzymatic glucose detection, Sens. Actuators, B 255 (2018) 1983–1994.

[15] G. Chang, H. Shu, Q. Huang, M. Oyama, K. Ji, X. Liu, Y. He, Synthesis of highly dispersed Pt nanoclusters anchored graphene composites and their application for non-enzymatic glucose sensing, Electrochim. Acta 157 (2015) 149–157.

[16] H. Shu, G. Chang, J. Su, L. Cao, Q. Huang, Y. Zhang, T. Xia, Y. He, Single-step electrochemical deposition of high performance Au-graphene nanocomposites for nonenzymatic glucose sensing, Sens. Actuators B: Chem. 220 (2015) 331–339.

[17] L. Shahhoseini, R. Mohammadi, B. Ghanbari, S. Shahrokhian, Ni(II) 1D-coordination polymer/C60-modified glassy carbon electrode as a highly sensitive non-enzymatic glucose electrochemical sensor, Appl. Surf. Sci. 478 (2019) 361–372.

[18] B.Z. Lu, L. Guo, F. Wu, Y. Peng, J.E. Lu, T.J. Smart, N. Wang, Y.Z. Finfrock, D. Morris, P. Zhang, N. Li, P. Gao, Y. Ping, S.W. Chen, Ruthenium atomically dispersed in carbon outperforms platinum toward hydrogen evolution in alkaline media, Nat. Commun. 10 (2019) 631.

[19] Y.i. Peng, B. Lu, S. Chen, Carbon-supported single atom catalysts for electrochemical energy conversion and storage, Adv. Mater. 30 (48) (2018) 1801995.

[20] A. Wang, J. Li, T. Zhang, Heterogeneous single-atom catalysis, Nat. Rev. Chem. 2 (6) (2018) 65–81.

[21] H.-J. Qiu, Y. Ito, W. Cong, Y. Tan, P. Liu, A. Hirata, T. Fujita, Z. Tang, M. Chen, Nanoporous graphene with single-atom nickel dopants: an efficient and stable catalyst for electrochemical hydrogen production, Angew. Chem. Int. Edit. 54 (2015) 14031–14035.

[22] C. Zhu, S. Fu, J. Song, Q. Shi, D. Su, M.H. Engelhard, X. Li, D. Xiao, D. Li, L. Estevez, D. Du, Y. Lin, Self-assembled Fe–N-doped carbon nanotube aerogels with single-atom catalyst feature as high-efficiency oxygen reduction electrocatalysts, Small 13 (2017) 1603407.

[23] G. Gao, Y. Jiao, E.R. Waclawik, A. Du, Single Atom (Pd/Pt) supported on graphitic carbon nitride as an efficient photocatalyst for visible-light reduction of carbon dioxide, J. Am. Chem. Soc. 138 (2016) 6292–6297.

[24] Y. Chen, S. Ji, Y. Wang, J. Dong, W. Chen, Z. Li, R. Shen, L. Zheng, Z. Zhuang, D. Wang, Y. Li, Isolated single iron atoms anchored on N-doped porous carbon as an efficient electrocatalyst for the oxygen reduction reaction, Angew. Chem. Int. Edit. 56 (2017) 6937–6941.

[25] L. Zhao, Y. Zhang, L.-B. Huang, X.-Z. Liu, Q.-H. Zhang, C. He, Z.-Y. Wu, L.-J. Zhang, J. Wu, W. Yang, L. Gu, J.-S. Hu, L.-J. Wan, Cascade anchoring strategy for general mass production of high-loading single-atomic metal-nitrogen catalysts, Nat. Commun. 10 (2019) 1278.

[26] B. Bayatsarmadi, Y. Zheng, A. Vasileff, S.-Z. Qiao, Recent advances in atomic metal doping of carbon-based nanomaterials for energy conversion, Small 13 (2017) 1700191.

[27] A. Han, W. Chen, S. Zhang, M. Zhang, Y. Han, J. Zhang, S. Ji, L. Zheng, Y. Wang, L. Gu, C. Chen, Q. Peng, D. Wang, Y. Li, A Polymer encapsulation strategy to synthesize porous nitrogen-doped carbon-nanosphere-supported metal isolated-single-atomic-site catalysts, Adv. Mater. 30 (2018) 1706508.

[28] T. He, B. Lu, Y. Chen, Y. Wang, Y. Zhang, J.L. Davenport, A.P. Chen, C.-W. Pao, M. Liu, Z. Sun, Nanowrinkled carbon aerogels embedded with FeN sites as effective oxygen electrodes for rechargeable zinc-air battery, Research 2019 (2019) 6813585.

[29] Y.X. Wang, H.Y. Su, Y.H. He, L.G. Li, S.Q. Zhu, H. Shen, P.F. Xie, X.B. Fu, G.Y. Zhou, C. Feng, D.K. Zhao, F. Xiao, X.J. Zhu, Y.C. Zeng, M.H. Shao, S.W. Chen, G. Wu, J. Zeng, C. Wang, Advanced electrocatalysts with single-metal-atom active sites, Chem. Rev. 120 (2020) 12217–12314.

[30] B.Z. Lu, Q.M. Liu, S.W. Chen, Electrocatalysis of single-atom sites: impacts of atomic coordination, Acs Catal. 10 (2020) 7584–7618.

[31] Y. Chen, S. Hu, F. Nichols, F. Bridges, S. Kan, T. He, Y.i. Zhang, S. Chen, Carbon aerogels with atomic dispersion of binary iron–cobalt sites as effective oxygen catalysts for flexible zinc–air batteries, J. Mater. Chem. A 8 (23) (2020) 11649–11655.

[32] A.L. Rinaldi, E. Rodríguez-Castellón, S. Sobral, R. Carballo, Application of a nickel hydroxide gold nanoparticles screen-printed electrode for impedimetric sensing of glucose in artificial saliva, J. Electroanal. Chem. 832 (2019) 209–216.

[33] T. He, Y.i. Peng, Q. Li, J.E. Lu, Q. Liu, R. Mercado, Y. Chen, F. Nichols, Y.i. Zhang, S. Chen, Nanocomposites based on ruthenium nanoparticles supported on cobalt and nitrogen-codoped graphene nanosheets as bifunctional catalysts for electrochemical water splitting, ACS Appl. Mater. Interfaces 11 (50) (2019) 46912–46919.

[34] B. Lu, Q. Liu, F. Nichols, R. Mercado, D. Morris, N. Li, P. Zhang, P. Gao, Y. Ping, S. Chen, Oxygen reduction reaction catalyzed by carbon-supported platinum few-atom clusters: significant enhancement by doping of atomic cobalt, Research 2020 (2020) 1–12.

[35] Z. Lu, B. Wang, Y. Hu, W. Liu, Y. Zhao, R. Yang, Z. Li, J. Luo, B. Chi, Z. Jiang, M. Li, S. Mu, S. Liao, J. Zhang, X. Sun, Isolated Zn-Co atomic pair for highly active and durable oxygen reduction, Angew. Chem. Int. Edit. 131 (2019) 2648–2652.

[36] P. Yin, T. Yao, Y. Wu, L. Zheng, Y. Lin, W. Liu, H. Ju, J. Zhu, X. Hong, Z. Deng, G. Zhou, S. Wei, Y. Li, Single cobalt atoms with precise N-coordination as superior oxygen reduction reaction catalysts, Angew. Chem. Int. Edit. 55 (2016) 10800–10805.

[37] A. Caglar, D. Düzenli, I. Onal, I. Tezsevin, O. Sahin, H. Kivrak, A novel experimental and density functional theory study on palladium and nitrogen doped few layer graphene surface towards glucose adsorption and electrooxidation, J. Phys. Chem. Solids 150 (2021) 109684.

[38] L.D. Burke, T.G. Ryan, The adatom/incipient hydrous oxide mediator model for reactions on silver in base, J. Appl. Electrochem. 20 (1990) 1053–1058.

[39] X. Wu, Y. Sun, T. He, Y. Zhang, G.-J. Zhang, Q. Liu, S. Chen, Iron, nitrogen-doped carbon aerogels for fluorescent and electrochemical dual-mode detection of glucose, Langmuir 37 (2021) 11309–11315.

[40] A. Caglar, D. Düzenli, I. Onal, I. Tezsevin, O. Sahin, H. Kivrak, A comparative experimental and density functional study of glucose adsorption and electrooxidation on the Au-graphene and Pt-graphene electrodes, Int. J. Hydrogen Energy 45 (2020) 490–500.

[41] G. Luo, Y.u. Jing, Y. Li, Rational design of dual-metal-site catalysts for electroreduction of carbon dioxide, J. Mater. Chem. A 8 (31) (2020) 15809–15815.

[42] H.-W. Lei, B. Wu, C.-S. Cha, H. Kita, Electro-oxidation of glucose on platinum in alkaline solution and selective oxidation in the presence of additives, J. Electroanal. Chem. 382 (1-2) (1995) 103–110.

[43] C. Xiong, L. Tian, C. Xiao, Z. Xue, F. Zhou, H. Zhou, Y. Zhao, M. Chen, Q. Wang, Y. Qu, Y. Hu, W. Wang, Y. Zhang, X. Zhou, Z. Wang, P. Yin, Y.u. Mao, Z.-Q. Yu, Y. Cao, X. Duan, L. Zheng, Y. Wu, Construction of highly accessible single Co site catalyst for glucose detection, Sci. Bull. 65 (24) (2020) 2100–2106.

[44] J. Chen, H. Yin, J. Zhou, L. Wang, J. Gong, Z. Ji, Q. Nie, Efficient nonenzymatic sensors based on Ni-MOF microspheres decorated with au nanoparticles for glucose detection, J. Electron. Mater. 49 (8) (2020) 4754–4763.

[45] N. Yang, K. Guo, Y. Zhang, C. Xu, Engineering the valence state of ZIF-67 by Cu2O for efficient nonenzymatic glucose detection, J. Mater. Chem. B 8 (14) (2020) 2856–2861.

[46] G. Zang, W. Hao, X. Li, S. Huang, J. Gan, Z. Luo, Y. Zhang, Copper nanowires-MOFs-graphene oxide hybrid nanocomposite targeting glucose electro-oxidation in neutral medium, Electrochim. Acta 277 (2018) 176–184.

[47] A. Ngamaroonchote, Y. Sanguansap, T. Wutikhun, K. Karn-orachai, Highly branched gold–copper nanostructures for non-enzymatic specific detection of glucose and hydrogen peroxide, Microchim. Acta 187 (2020) 559.

[48] J. Ye, D. Deng, Y. Wang, L. Luo, K. Qian, S. Cao, X. Feng, Well-aligned Cu@C nanocubes for highly efficient nonenzymatic glucose detection in human serum, Sens. Actuators, B 305 (2020) 127473.

[49] M. Wang, D. He, M. Huang, X. Wang, P. Jiang, In situ growth of Ni-B nanoparticles on Ni foam: an efficient 3D integrated anode for enzyme-free glucose detection, J. Alloys Compd. 786 (2019) 530–536.